

Molecular Signature and Activationless Transport in Cobalt-Terpyridine-Based Molecular Junctions

Quyên van Nguyen, Ushula Tefashe, Pascal Martin,* Maria Luisa Della Rocca, Frederic Lafolet, Philippe Lafarge, Richard L. McCreery, and Jean-Christophe Lacroix*

Cobalt terpyridine oligomers are compared with π -conjugated and ruthenium-centered layers in molecular junctions (MJs) with identical contacts. A wide range of layer thickness is investigated, and attenuation plots are obtained. Strong dependence of charge transport on molecular layers is found with a variation of four orders of magnitude of current density (J) for different molecules and $d = 7$ nm. For a Ru(bpy)₃ complex and bis-thienylbenzene MJs, the attenuation plot shows two different regions corresponding to two different dominant transport mechanisms. On the contrary Co(tpy)₂ and viologen-based MJs show no transition thickness in the attenuation plot, indicating a possible change of mechanism with film thickness, and very low attenuation factors (β of 0.17 and 0.25 nm⁻¹ from 2 to 14 nm, respectively). These β values indicate highly efficient long-range transport. This is attributed to the fact that the energy levels of the frontier orbital involved in transport are between, and thus almost in resonance with, the Fermi levels of the electrodes. Temperature-dependence measurements suggest that field ionization followed by multistep hopping and redox events can occur above 100 K, while the activationless region at low T indicates incoherent tunneling between redox sites with reorganization concerted with charge transfer.

1. Introduction

In molecular junctions (MJs), several types of molecules have been investigated, including purely organic compounds,^[1–5] proteins,^[5] and more recently complex clusters based on silicon^[6,7] or germanium,^[7] as well as organometallic compounds and inorganic complexes.^[8–16] Usually, in the tunneling regime, the rate of charge transport depends very much on the length of the organic molecule, and the values of the attenuation factor, β , for saturated molecules are from 5 to 10 nm⁻¹ whereas β values are in between 2 and 3 nm⁻¹ for π -conjugated molecules.^[1,2,5,17] A few exceptions have been found; for instance, nearly length-independent conductance is observed in polyporphyrin molecular wires,^[18] porphyrin nanorods,^[19] and extended viologen molecules,^[20] and there is no exponential length dependence of conductance reported for iodide-terminal oligothiophene single-molecule tunneling junctions.^[21]

In addition to organics, organometallic compounds and inorganic complexes are multifunctional molecules with many interesting electrochemical and photophysical properties that can be used in MJs to add new functionalities, such as light emission,^[8] photovoltaic effect,^[13] conductance switching^[12] for resistive memory,^[22–24] and Coulomb blockade.^[25] In 2003, using a cross-wire tunnel junction, Shashidhar and co-workers first showed that the conductance of MJs incorporating a platinum(II) complex was higher than that of oligo(phenylene ethylene) (OPE) MJs.^[26] Since then the conductance of other organometallic-based MJs has been investigated by several techniques, such as scanning tunneling microscope break junction (STM-BJ),^[27] conductive probe atomic force microscope (CP-AFM),^[14,28] Hg liquid drop,^[29] and mechanically controlled break junction (MCBJ).^[11] For example, using CP-AFM, Frisbie and co-workers found the first evidence that the β value of an organometallic (platinum(II))-based junction is much smaller ($\beta = 0.9$ nm⁻¹) than that of an organic-based junction in the same range of thickness.^[14,28] Small β values were also found in metal-centered MJs containing porphyrin units.^[27,30,31] Rampi and co-workers also reported that the β values of metal-centered MJs are much smaller than those of organic compounds and showed that they depend on the identity of the metal ion.^[29] An important result from this group is that β for a cobalt complex is 0.01 nm⁻¹ whereas it is 0.28 nm⁻¹ for an iron complex.

Dr. Q. van Nguyen, Dr. P. Martin, Dr. F. Lafolet, Prof. J.-C. Lacroix
ITODYS
Université de Paris
CNRS, UMR 7086, 15 rue J-A de Baïf, 75205 Paris, Cedex 13, France
E-mail: martin@univ-paris-diderot.fr; lacroix@univ-paris-diderot.fr

Dr. Q. van Nguyen
Department of Advanced Materials Science and Nanotechnology
University of Science and Technology of Hanoi (USTH)
Vietnam Academy of Science and Technology
18 Hoang Quoc Viet, Cau Giay, Hanoi, Vietnam

Dr. U. Tefashe, Prof. R. L. McCreery
Department of Chemistry
University of Alberta
11227 Saskatchewan Dr., Edmonton, AB T6G 2G2, Canada

Dr. M. L. Della Rocca, Prof. P. Lafarge
Laboratoire Matériaux et Phénomènes Quantiques (MPQ)
Université de Paris
CNRS, UMR 7162, 75205 Paris, Cedex 13, France

 The ORCID identification number(s) for the author(s) of this article can be found under <https://doi.org/10.1002/aelm.201901416>.

DOI: 10.1002/aelm.201901416

Several efforts have been made to compare the conductance of organic molecular MJs and metal-centered MJs directly and to establish the relationship between possible redox events in organometallic compounds or inorganic complexes and their conductance.^[9,10,32–35] However, the change in the conductance is usually attributed to the difference in the length of the molecule or to the strength of the electronic coupling between the contact and the molecule. It is rarely related to the redox events that may occur in such metal-centered MJs despite the fact that many studies indicate that metal centers enable the molecule energy level to be tuned relative to the Fermi energy levels of the electrodes.^[11,32] For example, Davidson et al. reported that the conductance of a single complex based on terpyridine is independent of the redox potential of the metallic core.^[34] We also note that studies on transport in organometallic and metal-centered MJs are usually limited to systems where the distance between the two electrodes is small (below 5 nm) and, consequently, understanding the long-range transport regime (thicknesses from 5 to 20 nm) is still a challenge.

The current report is focused on new cobalt-centered MJs and compares its transport properties to that of ruthenium-centered MJs and to two aromatic organic MJs lacking a metal center. Several molecular compounds were synthesized as shown in **Figure 1a** and then incorporated between two metallic electrodes.

The cobalt complex, namely $[\text{Co}(\text{tpy})_2](\text{PF}_6)_2$, consists of a cobalt(II) high-spin system at room temperature^[36] bonded to two terpyridine ligands bearing an aniline side group. It has a low highest occupied molecular orbital (HOMO)–lowest unoccupied molecular orbital (LUMO) gap (see Table S1 in the Supporting Information for the energy of the HOMO and LUMO of the used molecules) due to the cobalt-centered HOMO and LUMO orbitals.^[37,38] The Ru complex is $[\text{Ru}(\text{bpy})_3](\text{PF}_6)_2$ which was already studied in carbon-based MJs and showed robust bipolar light emission and charge transport.^[8] Its HOMO is much lower than that of $[\text{Co}(\text{tpy})_2](\text{PF}_6)_2$, and its LUMO orbital, centered on the bipyridine ligands, is much higher. The first organic compound examined here consists of donor molecules, namely bis-thienylbenzene

(BTB), oligomers with relatively high-energy HOMO. This layer can be easily p-doped at 0.5–0.6 V versus a saturated calomel electrode (SCE) and switched between an insulating and a conductive state.^[39–43] The second nonmetallic molecule is an electron acceptor, which incorporates a viologen unit namely 1-(4-phenyl)-1-methyl-4,4'-bipyridinium bis-hexafluorophosphate (VIOC1), with low-energy LUMO which can be easily reduced at –0.2 to 0.3 V/SCE.^[44–47] The molecular layers are all redox active, and strongly differ in their frontier orbital energies. MJs for all four molecules were fabricated by the same process, and all MJs have identical junction structure and contacts. The layers are deposited by diazonium cation reduction on Au substrates followed by direct vapor deposition of a top contact of titanium and Au which is an established and reproducible procedure for fabricating large-area devices with high yield.^[41,43,48,49]

The approach is directed at several questions about transport in large-area MJs. First, can cobalt complexes be incorporated in diazonium-derived MJs with yield and performance comparable to previously studied aromatic molecules or ruthenium complexes? Second, does transport in the four different systems fabricated by the same process with identical junction structure and contacts differ significantly from each other and show obvious molecular signature? Third, how is transport affected by the frontier orbitals of the cobalt-based layer in both the tunneling regime (thickness, d , less than 5 nm) and over greater distances? As an exciting result, highly efficient long-range transport properties were obtained with cobalt-based MJs.

2. Results

The cyclic voltammograms (CVs) of the two complexes in acetonitrile solution are shown in **Figure 2a**. The CV of $\text{Ru}(\text{bpy})_3$ in acetonitrile (red curves) exhibits three reversible reduction waves at –1.3, –1.6, and –1.8 V/SCE which can be attributed to the reduction of the three bipyridyl ligands.^[50–52] The irreversible oxidation peak at 1 V/SCE can be attributed to the oxidation

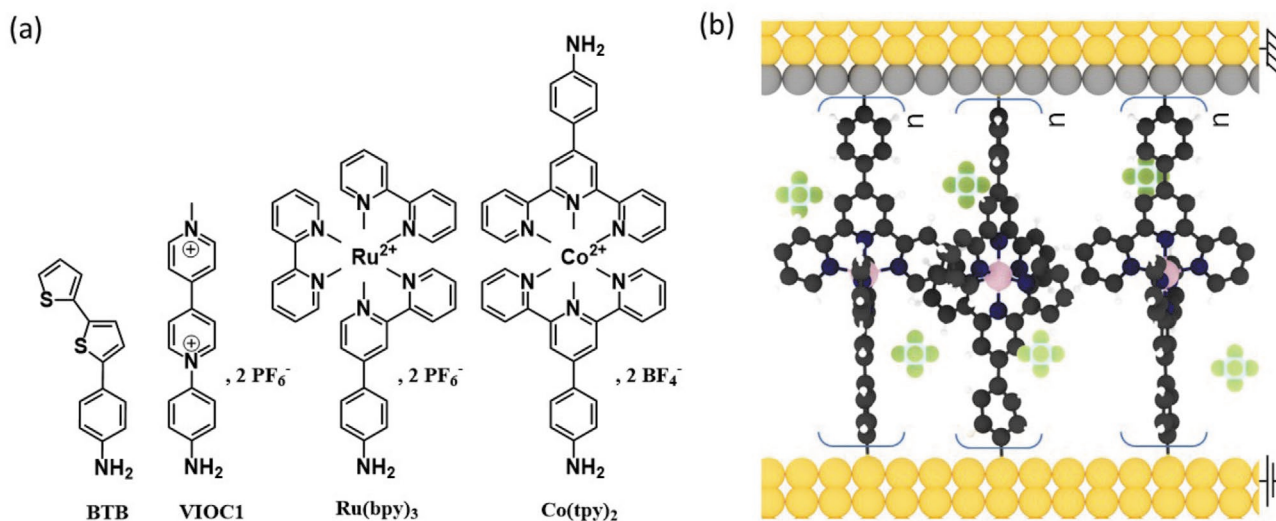


Figure 1. a) Chemical structure of the used organic molecules and inorganic complexes. b) Schematic illustration of a molecular junction based on $\text{Co}(\text{tpy})_2$ molecule.

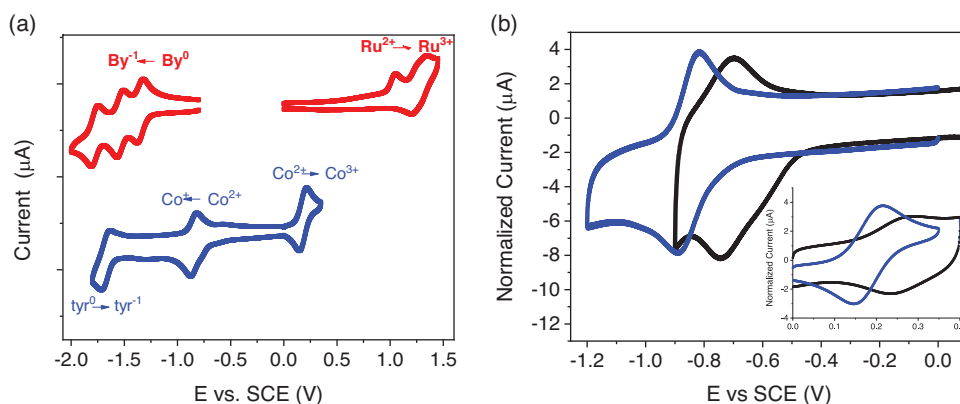


Figure 2. a) Cyclic voltammograms (CV) of $\text{Ru}(\text{bpy})_3$ and $\text{Co}(\text{tpy})_2$ in solution ($5 \cdot 10^{-4}$ M in acetonitrile (ACN) with 0.1 M tertbutyl ammonium hexafluorophosphate (TBAPF_6) at 0.1 V s^{-1} scan rate. b) CV in the negative potential range of $\text{Co}(\text{tpy})_2$ in solution (blue) and grafted on carbon electrode (black) in ACN. Inset: CV in the positive potential of $\text{Co}(\text{tpy})_2$ in solution (blue) and grafted on carbon electrode (black); in 0.1 M TBAPF_6 ACN solution, scan rate 0.1 V s^{-1} .

of the NH_2 group and the reversible peak at 1.25 V/SCE is due to the oxidation of Ru(II) to Ru(III).^[52] The CV of $\text{Co}(\text{tpy})_2$ (blue curves) shows a peak at 0.2 V/SCE which we assign to the oxidation of Co(II) to Co(III).^[37,38] The first reduction peak at -0.85 V/SCE can be assigned to the reduction of Co(II) into Co(I) while reduction of the terpyridyl ligand appears at -1.8 V/SCE.^[37,38] The main difference between $\text{Co}(\text{tpy})_2$ and $\text{Ru}(\text{bpy})_3$ is that the Co(II) core can be oxidized at 0.2 V/SCE and reduced at -0.85 V/SCE whereas the Ru core in $\text{Ru}(\text{bpy})_3$ oxidizes at 1.25 V/SCE, but cannot be reduced in the potential range examined.

The inorganic complexes were grafted onto a glassy carbon or Au substrate by in situ diazonium ion generation and electroreduction, as described previously.^[8,49,51] In general, a certain amount of *tert*-butyl nitrite (a few equivalents) was added to the solution of the amino metal complex and then the solution was incubated for 5 min in an inert atmosphere. The color of the solution changes during this time indicating the formation of the diazonium ion. The details of the in situ generation are provided in Table S2 (Supporting Information). For example, when 10 equivalents of *tert*-butyl nitrite were added to $\text{Co}(\text{tpy})_2$ solution, the red solution became brighter red. Voltammetric reduction of the diazonium solution (shown in Figures S1 and S2b in the Supporting Information for $\text{Co}(\text{tpy})_2$ and $\text{Ru}(\text{bpy})_3$,

respectively) then generates the phenyl radical which bonds to the surface. The electroactivity of a $\text{Co}(\text{tpy})_2$ -functionalized carbon electrode is shown in Figure 2b while that of $\text{Ru}(\text{bpy})_3$ is given in Figure S2b (Supporting Information). The oxidation peak of Co(II) to Co(III) appears at 0.3 V/SCE, which is slightly higher than for the amine in solution, and the reduction peak of Co(II) to Co(I) appears at -0.7 V/SCE, which is slightly less negative than in solution. These shifts are probably due to the loss on the amino groups in the grafting process. Overall the electrochemical HOMO–LUMO gap of the $\text{Co}(\text{tpy})_2$ grafted layer is close to 1 V and much lower than that of $\text{Ru}(\text{bpy})_3$, which is 2.7 V.

The survey and high-resolution X-ray photoelectron spectroscopy (XPS) of Co and N for the $\text{Co}(\text{tpy})_2$ layer on an Au substrate are shown in Figure 3a–c. The single well-defined N 1s peak at 400.1 eV in the high-resolution spectra rules out measurable azo-bridged grafting and is assigned to the aromatic nitrogen in the terpyridyl ligand.^[49,51–53] The photoelectron spectrum of Co 2p is shown in Figure 3b. The binding energies of $\text{Co}_{2p_{3/2}}$ and $\text{Co}_{2p_{1/2}}$ are observed at 781.2 and 796.6 eV, respectively, and are separated by a significant spin–orbit splitting (ΔE) of 15.4 eV. These results are in good agreement with the literature for Co(II) complexes.^[54,55] The N/Co, P/F, and

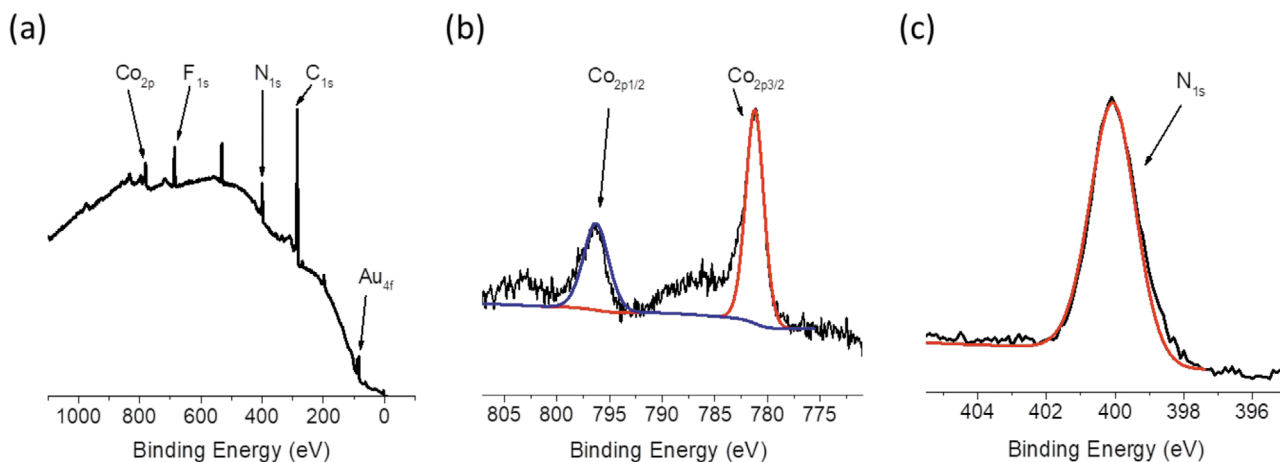


Figure 3. a) survey XPS of $\text{Co}(\text{tpy})_2$ -functionalized gold electrodes and high-resolution XPS spectra of b) Co 2p and c) N 1s.

P/Co ratios are 5.8, 5.3, and 1.8, respectively, which are very close to the theoretical values of 6.0, 6.0, and 2.0, respectively. This XPS evidence indicates that the $\text{Co}(\text{tpy})_2$ functionalized on the Au substrate has the expected stoichiometry and includes negligible formation of azo groups. Importantly, the P/Co ratio indicates that around two PF_6 anions are incorporated in the layer, as depicted in Figure 1b, and confirms that the cobalt centers are mainly in a +II oxidation state. XPS analysis of the $\text{Ru}(\text{bpy})_3$ films formed on Au via in situ diazonium generation was already reported^[8] and confirms that the molecular layers have the composition and metal center oxidation state corresponding to those expected from the precursor structure.

Next, the diazonium electroreduction was performed on Au stripes (20 μm wide, a few centimeters long, and 45 nm thick) deposited by e-beam on Si/SiO₂ wafer. Thickness of the molecular layers was varied by changing the experimental conditions during electrochemical grafting, and AFM measurements were used to measure the thickness with a previously described procedure.^[43,46,49] We found that the thickness of the $\text{Co}(\text{tpy})_2$ molecular layer can be changed from 2 to 20 nm by modifying the electrochemical conditions. Table S3 (Supporting Information) lists the electrochemical conditions used for varying the layer thicknesses examined.

MJs were then fabricated using complementary metal oxide semiconductor (CMOS)-compatible procedures described previously^[41,43,46,48,49] and summarized in Section S2 (Supporting Information). Several thicknesses of each inorganic complex layer were electrografted onto Au stripes, and the MJs were completed by direct vapor deposition of 2 nm of Ti and 45 nm of Au in a cross-bar geometry. Junction designations include subscripts indicating layer thicknesses in nanometers, with all devices using the same bottom and top contact electrodes. Complete MJs (Au/molecules/Ti/Au) will be designated by the molecular layers, including subscripts for layer thickness in nanometers. For example, $[\text{Co}(\text{tpy})_2]_{7\text{ nm}}$ means a 7 nm layer of $\text{Co}(\text{tpy})_2$ electrografted onto a bottom Au electrode (45 nm) followed by 2 nm of Ti and 45 nm of Au top contact deposited directly by e-beam evaporation in vacuum.

All metal-centered MJs were fabricated in high yield, i.e., above 90%, with more than 36 of 40 tested junctions for each molecular system and each thickness above 5 nm yielding non-shortened JV curves. Note that the total amount of MJs fabricated and tested for this study was ≈ 1000 (2 samples with 24 MJs each and 20 tested for each thickness) and also that fabrication yield of organic-based junction drops to 20% when the layer thickness is only 2 nm, while fabrication yield remains high (above 70%) when using 2–3 nm thick layers of complexes. Since 2–3 nm is close to the length of one molecule of $\text{Co}(\text{tpy})_2$ or $\text{Ru}(\text{bpy})_3$, the 2–3 nm devices are true monolayers.

Figure 4a,b compares the average JV curves of the two metal-centered MJs and the two organic-based MJs with similar thicknesses (7–8 nm). They are obtained by averaging the overlays of JV curves from 20 different MJs with the same thickness for each system ($[\text{Ru}(\text{bpy})_3]_{3-7\text{ nm}}$ and $[\text{Co}(\text{tpyr})_2]_{2-7\text{ nm}}$). We note that JV curves are nearly symmetric despite the fact that the electrodes are asymmetric (Au and Ti/Au), with the absolute value ratio of $J(+1\text{ V})/J(-1\text{ V})$ less than 2.0 in all cases. None of these metal-centered junctions significantly rectify the current, which is similar to the results obtained with VIOC1-based MJs^[46] but in marked contrast with those obtained with BTB-based MJ of similar thickness and using the same contacts which showed pronounced rectification properties at 2.7 V.^[41,43,49]

An important result is that the conductance of $[\text{Co}(\text{tpy})_2]_{7\text{ nm}}$ is much higher than that of all the other systems. For example, at 1 V the current density for $[\text{Co}(\text{tpy})_2]_{7\text{ nm}}$ ($\approx 0.25\text{ A cm}^{-2}$) is 250 times that of $[\text{Ru}(\text{bpy})_3]_{7\text{ nm}}$ (0.001 A cm^{-2}), even though the two compounds share similar coordination spheres. BTB MJ in this potential range is the least conductive system despite its structure based on long oligothiophene which favors charge delocalization while VIOC1, a molecule which incorporates localized redox centers, is much more conductive than BTB. These results confirm that for $d = 7\text{ nm}$, a strong molecular signature on transport is observed with $[\text{Co}(\text{tpy})_2]_{7\text{ nm}}$ being the most conductive layers used in this study and a variation of four orders of magnitude of J for different molecules at 1 V. Note that the large differences in conductance among the four

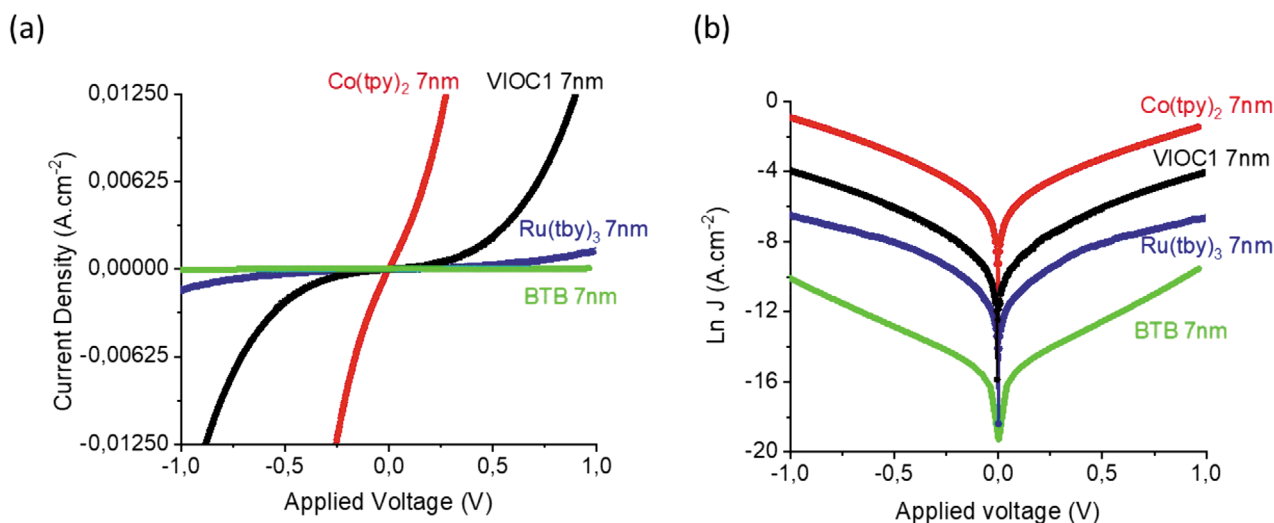


Figure 4. a) JV overlay of $[\text{Co}(\text{tpyr})_2]_{7\text{ nm}}$ (red), $[\text{VIOC1}]_{7\text{ nm}}$ (black), $[\text{Ru}(\text{bpy})_3]_{7\text{ nm}}$ (blue), and $\text{BTB}_{7\text{ nm}}$ green MJs. b) Same data in $\ln J$ format.

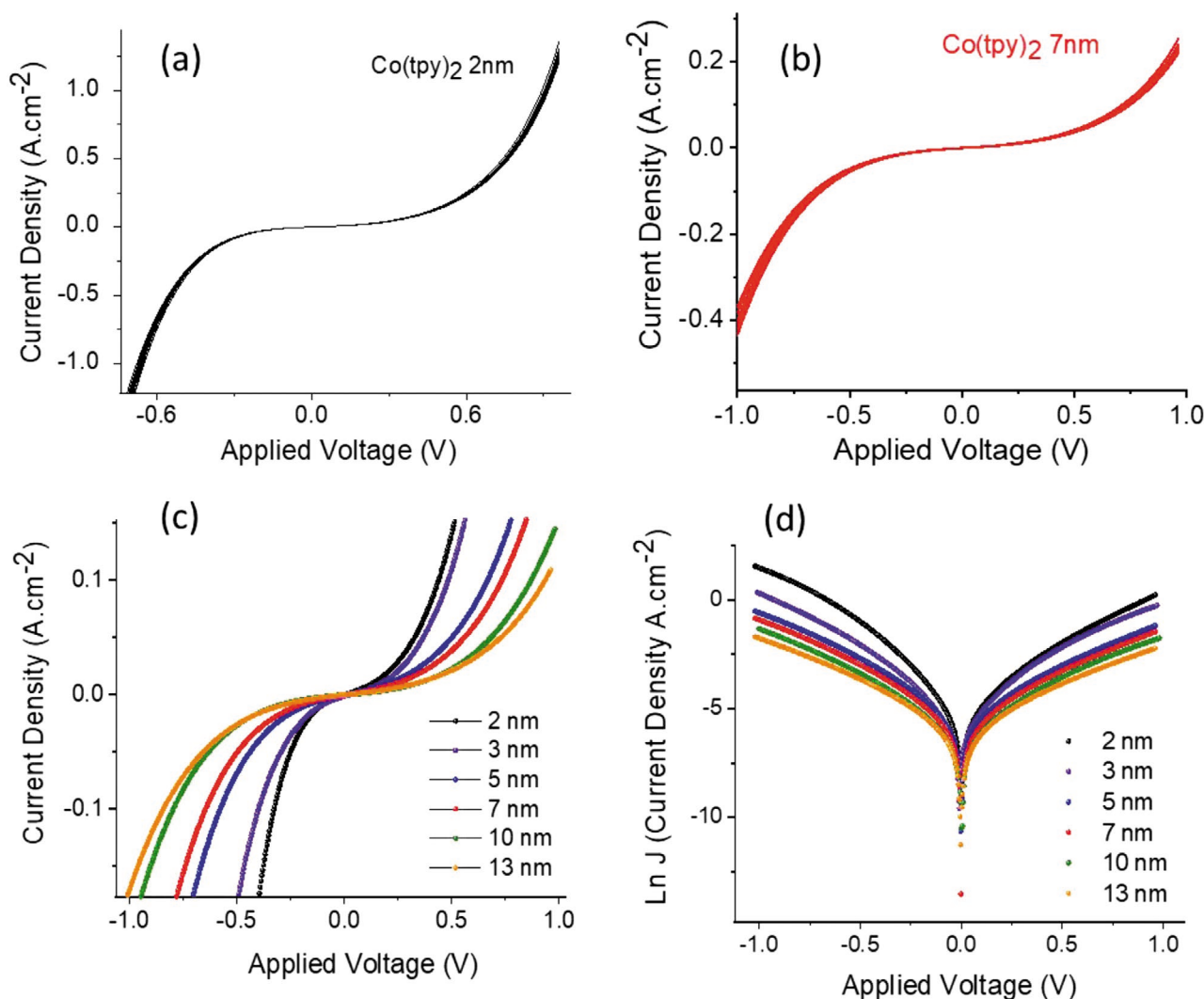


Figure 5. JV overlay of several $\text{Co}(\text{tpy})_2$ junctions for a) 2 nm (black) and b) 7 nm (red) thicknesses. c) Comparison of averaged JV curves of $\text{Co}(\text{tpy})_2$ for various thicknesses. d) Same data in $\ln J$ versus applied voltage.

molecules occur over the entire bias range depicted here, i.e., ± 1 V. These results stimulated consideration of $\text{Co}(\text{tpy})_2$ layers in more detail.

Figure 5a,b shows overlays of several JV curves of $\text{Co}(\text{tpy})_2$ MJs with the thickness noted in the figure (average of 40 different devices is shown for each thickness; see Figure S3 in the Supporting Information for other thicknesses). The JV curves of these devices are almost symmetric, and the standard deviations of J (1 V) are only 6% for $d = 2$ nm ($N = 40$) and 8% for $d = 7$ nm ($N = 40$). An additional $[\text{Co}(\text{tpy})_2]_{7\text{ nm}}$ JV curve from 40 MJs with error bars is shown in Figure S4 (Supporting Information). The small standard deviations of the current clearly demonstrate that the films are homogeneous, with acceptably uniform thicknesses, and that reproducibility of the MJ fabrication process is high. In addition, the current density in $[\text{Co}(\text{tpy})_2]_{2\text{ nm}}$ MJs (1.2 A cm^{-2} at 1 V) is just four times that of $[\text{Co}(\text{tpy})_2]_{7\text{ nm}}$ (0.25 A cm^{-2}). This observation is very interesting since for MJs based on π -conjugated organic compounds in the tunneling regime, the commonly reported β value of 2 nm^{-1}

should result in a decrease of more than four orders of magnitude if the thickness increases from 2 to 7 nm. Figure 5c shows an overlay of the average JV curves for six thicknesses of $\text{Co}(\text{tpy})_2$ ($N = 240$), with Figure 5d having the same data in $\ln J$ versus V format. It clearly shows a weak dependence of current density on thickness for $\text{Co}(\text{tpy})_2$ MJs. To directly visualize the effect of the thickness, $\ln J$ at 1 V versus molecular layer thickness for $\text{Co}(\text{tpy})_2$, $\text{Ru}(\text{bpy})_3$, and BTB is plotted in **Figure 6**, with that of VIOC1 from previous experiments included for comparison.^[46] Recall that all MJs in Figure 6 have the same device structure and represent a total of 1000 MJs. The β values equal to the slope of the attenuation plot are given for each system and provide insight into the dominant transport mechanism.

For BTB and $\text{Ru}(\text{bpy})_3$ devices, two distinguishable slopes are observed in the attenuation plot. BTB MJs with Au and Ti/Au contacts have two β values, 1.8 nm^{-1} for thickness from 2 to 5 nm and 0.36 nm^{-1} from 5 to 15 nm. The β value below 5 nm agrees well with those reported for aromatic structures in both single molecule and “ensemble” MJs, and is generally

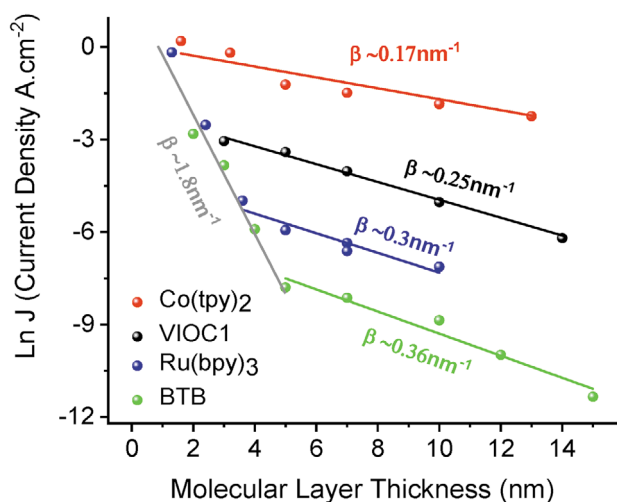


Figure 6. Attenuation plots taken at 1 V of MJs for different molecular units. β value is the slope of the curve and is indicated for each molecule.

attributed to “off-resonance tunneling.”^[2,3,56–62] Above 5 nm, a smaller β value is measured. Similar results were reported for BTB MJs fabricated with carbon contacts, where β is 2.9 nm^{-1} for thicknesses below 8 nm and 0.8 nm^{-1} for 8–16 nm.^[56] The marked difference in the transition thickness and β values of MJs based on BTB with different contacts may result from stronger electronic coupling at the carbon interface compared to the Au/molecule and Ti/molecule used here.

More interestingly, we found that $\text{Co}(\text{tpy})_2$ MJs show unique electrical properties. First, the current density measured for $\text{Co}(\text{tpy})_2$ MJs is always higher than that for VIOC1, $\text{Ru}(\text{bpy})_3$, and BTB MJs at a given bias. For instance, the current density of 13 nm $\text{Co}(\text{tpy})_2$ MJs at 1 V is more than 1000 times that of 12 nm BTB MJs. Second, as shown in Figure 6, we found that there is no transition point at which we observe a change in β . Moreover, the β value of $\text{Co}(\text{tpy})_2$ MJs is very small (0.17 nm^{-1}) and is weakly bias dependent (Figure S5, Supporting Information). This is among the smallest values obtained in large-area MJs and demonstrates highly efficient long-range transport in $\text{Co}(\text{tpy})_2$ -based MJs. Small β values have been observed in MJs based on porphyrin units; for instance, Bruce et al. reported recently a β value of 0.6 nm^{-1} for conjugated (porphinato)–zinc

MJs.^[30] Note also that Tuccitto et al. were the first ones to report close to zero β value for cobalt-based MJs, whose thickness was restricted to 40 nm.^[29]

To explore in more detail the transport mechanism in $\text{Co}(\text{tpy})_2$ MJs, temperature dependence (from 7 to 290 K) of *JV* behavior was obtained for several 7 nm $\text{Co}(\text{tpy})_2$ MJs, a thickness above that of the direct tunneling regime. These MJs are stable during the cooling or heating process, and several temperature excursions could be performed on a given device. Figure 7a shows *JV* curves for a single $\text{Co}(\text{tpy})_2$ junction from 7 to 300 K. The *JV* curves are nearly symmetric at all temperatures. Arrhenius plots derived from these *JV* curves at two different bias values (Figure 7b) provide activation barrier energies (E_a). The Arrhenius plots of $\ln J$ versus $1000/T$ are qualitatively like those reported previously for BTB with carbon contacts,^[56] or for VIOC1 with Au and Ti/Au contacts, with an activated region between 100 and 300 K, and a nearly activationless region below 100 K.^[46] At high temperature, E_a is $\approx 80 \text{ meV}$ and decreases with electric field while, below 100 K, E_a is less than 1 meV. These values clearly indicate that at room temperature, an activated mechanism is involved in the transport process but rules out several electron transport mechanisms, such as interchain redox hopping, which have typical E_a above 200–300 meV.^[59,61,63] The small E_a below 100 K ($<1 \text{ meV}$) indicates that tunneling occurs and that transport is not only due to classical charge transfer with reorganization preceding electron transport.

Such a small activation energy is rarely reported for film thickness above 5 nm, and it is only recently that the activation energies in BTB,^[41,56] VIOC1,^[46] and fluorene and nitroazobenzene^[64,65] molecular junctions with thicker films were found to be less than 100 meV. This small activation energy was attributed to field ionization associated with intrachain transfer for BTB MJs with carbon contacts,^[56] and a multistep tunneling mechanism controlling electron transfer was proposed for fluorene MJs.^[64] Note also that a recent study on self-assembled monolayer (SAM)-based large-area MJs proposed a Marcus inversion mechanism with transport being activationless for certain molecular structures in the range of 250–330 K and activated when additional aliphatic carbons were inserted in the conduction path.^[66] A recent report on thin MJs described how Marcus kinetics can become activationless at high bias, depending on the electronic coupling between molecules and contact.^[67]

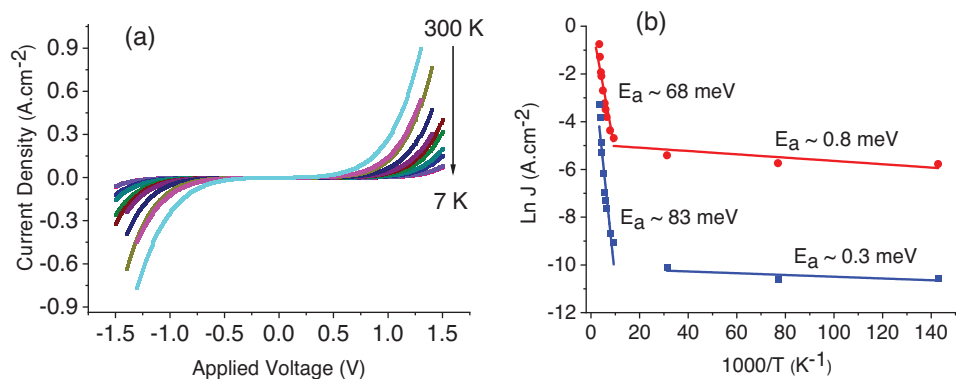


Figure 7. a) *JV* overlay of $[\text{Co}(\text{tpy})_2]_7 \text{ nm}$ MJs at different temperature dependences. b) Arrhenius plot of $\ln J$ versus $1000/T$ taken at 0.5 V (blue) and 1 V (red).

3. Discussion

As stated in the “Introduction,” this study addresses several questions about transport in large-area MJJs. First, our results show that cobalt and ruthenium complexes can be incorporated in diazonium-derived MJJs with yield and performance being comparable to previously studied organic aromatic molecules. As an exciting result, using these inorganic complexes, it seems to be possible to stop the growth of the film deposited by diazonium electroreduction at the monolayer level thanks to the steric effect of the bipyridine or terpyridine ligands. This is a clear advantage compared to MJJs based on organic diazonium precursors, where it remains difficult to stop the growth at the monolayer level. Fabrication yields are also better for metal-centered devices incorporating 2–3 nm thick layers. Second, transport in the four different systems, fabricated by the same process with identical junction structure and contacts, differs significantly from each other and shows an obvious molecular signature. Third, in the present study, two groups of molecules which seem to behave in a similar way can be defined, Co(tpy)₂ and VIOCl compared to Ru(bpy)₃ and BTB. Each group contains one organic molecule and one inorganic complex. As a consequence, there is no clear distinction between metal-centered and organic-based MJJs in both the tunneling regime (thickness, *d*, less than 5 nm) and over greater distances.

For BTB and Ru(bpy)₃ MJJs, there are two distinguishable slopes in the attenuation plot, indicating a change in the dominant transport mechanism at a transition thickness, *d*_{trans}. *d*_{trans} for BTB is around 5 nm while that of Ru(bpy)₃ MJJs is around 3.5 nm. Interestingly, for thicknesses below *d*_{trans}, all the points lie on the same line with the same slope, whatever the molecule used (Figure 6). These results are consistent with non-resonant tunneling being the dominant mechanism for thicknesses below *d*_{trans}.^[57] When the thickness increases, a new transport mechanism is operative. Above *d*_{trans}, the β values of Ru(bpy)₃ and BTB are close (0.3 and 0.36 nm⁻¹, respectively) and are smaller than those observed for Ru(bpy)₃ and BTB MJJs using carbon contacts (0.6 and 0.8 nm⁻¹, respectively).^[8,56,68] BTB-based MJJs' transport above *d*_{trans} was attributed to field-induced ionization associated with activationless intrachain hopping,^[56] and in Ru(bpy)₃ MJJs with *e*C contact, light emission was observed when the thickness was above 5 nm, which was attributed to bipolar transport and redox events.^[8,68] Above the transition thicknesses, charge injection into molecular orbitals or redox events inside the junctions is thus turned on, and transport is due to electron transfer between redox centers and involves mainly intrachain hopping. The absence of observable activation at low temperature implies sequential or multistep tunneling and, possibly, depending on the time scale, reorganization concerted with charge transfer.^[15,64] Within this framework, the smaller transition thicknesses for ruthenium-based MJJs compared to that observed in BTB-based MJJs can be understood in terms of size of charge carriers in these materials, which are known to be smaller in Ru-based mixed-valence compounds compared to oligothiophene polarons.^[69,70] It may also be strongly affected by the large number of counterions in ruthenium-based MJJs, which can reduce the energetic threshold needed to turn on charge injection in molecular orbitals or redox events in the solid state junction.

In contrast, VIOCl and Co(tpy)₂ MJJs show highly efficient long-range transport associated with small β values of 0.25 and 0.17 nm⁻¹ with no transition between two transport regimes in the investigated thickness range. On the basis of these observations, we can state that direct off-resonant tunneling has a small contribution in VIOCl and Co(tpy)₂ MJJs and is not the dominant transport mechanism in these MJJs at all investigated thicknesses (3–14 nm). Direct tunneling may only apply below 3 nm for VIOCl MJJs. Several examples in the literature have reported highly efficient long-range transport with small β values. Koliwoška et al. reported that in single-molecule MJJs based on extended viologen compounds, the β value is 0.06 nm⁻¹ for thicknesses from 2 to 11 nm, which they attributed to phase-coherent tunneling.^[20] A low β of 0.4 nm⁻¹, associated with a strong dependence on temperature (*E*_a above 300 K between 80 and 220 meV) has also been reported for porphyrin oligomers.^[27,71] Despite this activation energy, usually indicating transport by activated hopping, the observed temperature and length dependence were also shown to be consistent with phase-coherent tunneling.^[27,71] Efficient long-range transport due to resonant charge transport in single porphyrin molecular wires^[18] or via proteins was recently reported.^[72,73] In the present case, the HOMO level of Co(tpy)₂ is close to the Fermi level of Au, a situation which clearly favors on-resonant tunneling and could explain the low β value (in the Simmons model β depends on the square root of the tunneling barrier, and by decreasing the gap between the HOMO and the Fermi level of the contacts decreases β). However, intrachain hopping is also known to give low β values, and ionic species in Co(tpy)₂-based MJJs may enhance the electron injection rate at the interfaces and trigger hopping as the dominant mechanism at unusually low thicknesses.

Two different dominant mechanisms can thus be considered to explain the highly efficient long-range transport in Co(tpy)₂ MJJs, namely, on-resonant tunneling^[20,27,71] and intrachain hopping based on redox events.^[56] Note that the latter one implies multistep or sequential tunneling inside the molecular layer at low *T* with reorganization concerted with or following electron transfer. Note also that these two mechanisms are not mutually exclusive. The values of the activation energy measured for VIOCl and Co(tpy)₂ MJJs are quite similar (70 meV Co(tpy)₂ and 90 meV for VIOCl above 150 K at 1 V), but transport is activationless below 150 K in both cases. This suggests near-resonant tunneling as the plausible transport process at low *T* but indicates that at room temperature, an activated mechanism is involved in addition to nonresonant tunneling.

Co(tpy)₂ and VIOCl MJJs thus behave in a very similar way. They also share a specific feature that makes them different from BTB and Ru(bpy)₃. The HOMO energy levels of Co(tpy)₂ estimated from electrochemical data are very close (–4.8 eV) but above that of gold (–5.1 eV). The LUMO energy level of VIOCl is also very close (–4.5 eV) but below the Fermi level of Ti (–4.1 eV). Hence, in both cases the frontier orbital levels of the molecules involved in transport (in vacuum) are between the Fermi levels of the two electrodes. This situation is depicted in **Figure 8a** for Co(tpy)₂ MJJs.

In the MJJs studied, strong electronic coupling at both interfaces is expected, and the Co(tpy)₂ HOMOs are significantly broadened as depicted in **Figure 8b**. Moreover, at zero bias, the

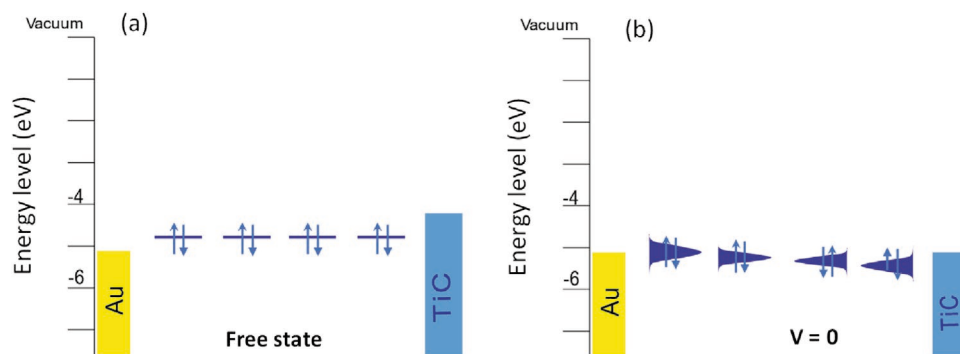


Figure 8. Energy diagram of Au/Co(tpy)₂/Ti/Au MJs a) in the free state and b) connected in an MJ at zero bias. The number of orbital energy levels in the Co(tpy)₂ layer is arbitrary.

HOMO of Co(tpy)₂ cannot remain between the Fermi levels of the isolated Au or the Ti electrodes once the MJ is assembled. An electrochemical equilibrium must occur, so that the Co(tpy)₂ HOMO and the Fermi level of Au are nearly aligned (Figure 8b, left electrode), which promotes a mixed valence situation in the MJs even though no bias is applied. A similar situation occurs in VIOC1 MJs.^[46] As a consequence, when a bias is applied, and independently of its polarization, it is always favorable to inject holes into the Co(tpy)₂ as there will always be a specific molecular level of the layer at tunneling distance (below 5 nm) in resonance with the Fermi level of one electrode, so that there will be a high current density between the two electrodes with no preferred direction. Furthermore, in this situation the dominant transport mechanism depends little on thickness, and intrachain activated hopping and multistep tunneling between redox centers can participate at unusually low thicknesses because of the mixed valence situation^[70] generated in the layer at one of the interfaces. This interpretation is supported by ultraviolet photoelectron spectroscopy (UPS) measurements of the valence band spectra which show (Figure S7, Supporting Information) a large density of states close to the Fermi energy of gold with a very small injection barrier (less than 0.3 eV). It is also supported by the recent work on plasmonic tunnel junction in which a transition from coherent to hopping electron transport was evidenced in single-molecule junction, whose thickness is close to 1 nm when biphenyl was replaced by viologen moieties. This study enabled the observation of redox processes in real time at the single molecular level despite the 1 nm distance between the two electrodes.^[74]

4. Conclusion

To summarize, several important remarks can be made. First, this study has compared π -conjugate-based and metal-centered MJs with identical contacts. It clearly shows that both types of molecules can behave similarly and can withstand high current densities and efficient long-range transport over distances up to at least 14 nm.

In particular, Co(tpy)₂ MJs, where the complex consists of Co(II) and terpyridinyl ligands, show important properties including a very low β value of 0.17 nm⁻¹, high current density, and no transition thickness in the attenuation plot expected for

a change in mechanism with film thickness. This β value is among the smallest attenuation factor reported to date in large-area molecular junction and indicates that long-range transport is highly efficient in Co(tpy)₂ MJs. Note also that VIOC1 MJs were shown to be quite similar to Co(tpy)₂ MJs with a β value of 0.25 nm⁻¹ despite a lower J_0 . Such properties can be partially attributed to the fact that the HOMO level of Co(tpy)₂ is between the Fermi level of Au and Ti, and thus almost in resonance with the Fermi level of the electrodes. However, transport in Co(tpy)₂ is clearly activated above 100 K with activation energies between 80 and 60 meV and decreases with increasing applied voltage or electric field. This activation energy indicates that resonant tunneling is not the only transport mechanism in Co(tpy)₂-based MJs and suggests that field ionization followed by multistep hopping possibly involving reorganization occurs. At high T , activated hopping between Co(tpy)₂ centers with reorganization preceding electron transfer may occur while activationless transport for VIOC1 and Co(tpy)₂ at temperature below 100 K implies that incoherent tunneling between redox sites occurs with reorganization concerted with or following charge transfer.

We also found that for BTB and Ru(bpy)₃ in Au/Ti MJs, the attenuation plots show two different regions corresponding to two dominant transport mechanisms. Below a transition distance, d_{trans} , nonresonant direct tunneling dominates and both molecules exhibit very similar conductances and β values. In other words, in the direct off-resonant tunneling regime, the conductances of MJs are almost independent of the molecule, which is in good agreement with previous studies.^[57,64] Above d_{trans} , a new mechanism is operative and overcomes direct tunneling. In this transport regime, the current densities through the MJs and the value of d_{trans} show a strong molecular signature. For example, the transition distance in BTB MJs is around 5 nm, while it is only 3.5 nm for Ru(bpy)₃ (and possibly below 3 nm in VIOC1 MJs). We propose that this transition is the onset of incoherent transport by field ionization leading to multistep tunneling and redox events occurring in the MJs despite the fact that they are solid-state devices. We also propose that the difference in d_{trans} between metal-centered MJs and π -conjugated MJs can be attributed to the size of the redox sites formed after injecting or removing the charge into or from the molecules. This transition is not observed with VIOC1 and Co(tpy)₂-based MJs because a mixed valence situation occurs

in these layers as a result of the electrochemical equilibrium at one of the interfaces which allows intrachain activated hopping and multistep tunneling between redox centers at unusually low thicknesses (below 3 nm).

5. Experimental Section

The bottom electrodes were fabricated using a gold stripe substrate (gold thickness 45 nm on a Ti 2 nm adhesion layer) on SiO₂/Si wafers with a width of 20 μm and several millimeters long. They were used for electrodeposition of the layers and after that an electron beam Ti/gold top contact was deposited as described in detail previously.^[41,43,46,48,49,75] Details are also provided in Section S2 (Supporting Information). Each sample allowed the fabrication of 24 molecular junctions with lateral dimensions of 20 by 20 μm (area: 4 × 10⁻⁶ cm²). A pressure of 10⁻⁸ Torr during Ti deposition was used to reduce oxidation of Ti from the residual oxygen and water of the vapor deposition systems but since reaction of Ti with the layers is likely, it was anticipated that Ti–C covalent bonds are generated at the molecule/top electrode interface as demonstrated in BTB-based MJs.^[43] For all junctions using different molecules, the Ti/Au top contact deposition was performed with identical conditions, and all junctions were also completed using lithography mask for top electrode deposition. A few junctions were fabricated using shadow mask for top electrode deposition. No significant differences were observed in JV curves compared to those recorded when top electrode deposition was done using lithography mask. This showed again that the fabrication techniques used here were fully compatible with standard microfabrication techniques.^[76]

All the molecules studied include a terminal aniline group which allows in situ diazonium generation using a well-described procedure with *tert*-butylnitrite (Aldrich) as a reagent.^[42,43,46,49,52] 1-(2-bisthiényl)-4-aminobenzene and 1-(4-aminophényl)-1'-methyl-4,4'-bipyridinium bis-hexafluorophosphate were synthesized using procedures adapted from the literature.^[39,40,45] After grafting on the Au surfaces and loss of their amino groups, the generated multilayers were named BTB and VI0C1 layers. [Ru(bpy)₂]²⁺(PF₆⁻)₂ was deposited from a phenyl diazonium derivative as already described.^[8] [Co(tpy)₂]²⁺(PF₆⁻)₂ oligomers were grafted from a cobalt complex bearing two 1-(4-aminophényl)-terpyridine ligands since the synthesis method used only allows symmetric cobalt complexes.^[37,38] CV recorded during grafting of Co(tpy)₂ and Ru(bpy)₃ layers was provided, as examples, in Figures S1 and S2a of Supporting Information, respectively.

Layer thicknesses were determined by AFM measurements. The thicknesses of the gold stripe deposited on SiO₂ and of the gold stripe covered by the grafted layer were measured, and the thickness of the layer was deduced by subtracting the gold thickness^[43,46,49] using a statistical procedure as shown in Figure S6 (Supporting Information). Standard deviations of thickness were in the range of 0.7–0.9 nm as indicated in Section S6 (Supporting Information). All thicknesses reported below were determined by AFM for each deposition condition and on a location on the bottom gold stripe less than 1 mm away from the position of the top electrode of the MJ.

Current density versus bias voltage (JV) characteristics were measured in air with a Keithley 2602b source meter at 2 V s⁻¹ or by dc polarizing the junction while measuring the current with a low-noise current amplifier. In each case, a two-probe setup configuration was used with the top electrode grounded while applying a bias to the bottom electrode. All JV curves in figures were obtained in air, and each curve presented in figures was an average JV curve obtained with all the MJs fabricated on each sample. Low-temperature measurements were performed using a variable temperature insert while keeping the sample in He atmosphere. The device was allowed to heat from 7 K to room temperature while successive JV curves were recorded.^[43,46]

XPS analyses was performed in ultrahigh vacuum system (ThermoFisher Scientific, K Alpha+) with a base pressure of 2 × 10⁻¹⁰ mbar. XPS was performed using an Al KR X-ray source (1486.6 eV) and a microfocused monochromatic and magnetic lens.

UPS analyses were performed on a modified gold substrate using a ThermoFischer Scientific K Alpha+ system with a base pressure of 2 × 10⁻¹⁰ mbar. The analyses were carried out using monochromatic He I (21.21 eV) emission together with a toroidal mirror monochromator.

Supporting Information

Supporting Information is available from the Wiley Online Library or from the author.

Acknowledgements

This work was supported the French Agence Nationale de la Recherche (ANR) under Grant ANR-15-CE09 0001-01 and by the University of Alberta, the National Research Council of Canada, the National Science and Engineering Research Council, and Alberta Innovates. ANR and CGI (Commissariat à l'Investissement d'Avenir) were also gratefully acknowledged for their financial support of this work through Labex SEAM (Science and Engineering for Advanced Materials and devices) ANR 11 LABX 086, ANR 11 IDEX 05 02.

Conflict of Interest

The authors declare no conflict of interest.

Keywords

diazonium electroreduction, electron transport, electronic materials, metal-centered molecular junctions, molecular electronics

Received: December 17, 2019

Revised: February 12, 2020

Published online: April 2, 2020

- [1] A. Vilan, D. Aswal, D. Cahen, *Chem. Rev.* **2017**, *117*, 4248.
- [2] D. Xiang, X. Wang, C. Jia, T. Lee, X. Guo, *Chem. Rev.* **2016**, *116*, 4318.
- [3] H. B. Akkerman, P. W. M. Blom, D. M. de Leeuw, B. de Boer, *Nature* **2006**, *441*, 69.
- [4] H. Jeong, D. Kim, D. Xiang, T. Lee, *ACS Nano* **2017**, *11*, 6511.
- [5] N. Amdursky, D. Marchak, L. Sepunaru, I. Pecht, M. Sheves, D. Cahen, *Adv. Mater.* **2014**, *26*, 7142.
- [6] H. Li, M. H. Garner, T. A. Su, A. Jensen, M. S. Inkpen, M. L. Steigerwald, L. Venkataraman, G. C. Solomon, C. Nuckolls, *J. Am. Chem. Soc.* **2017**, *139*, 10212.
- [7] T. A. Su, H. Li, R. S. Klausen, N. T. Kim, M. Neupane, J. L. Leighton, M. L. Steigerwald, L. Venkataraman, C. Nuckolls, *Acc. Chem. Res.* **2017**, *50*, 1088.
- [8] U. M. Tefashe, Q. Van Nguyen, F. Lafolet, J.-C. Lacroix, R. L. McCreery, *J. Am. Chem. Soc.* **2017**, *139*, 7436.
- [9] S. Bock, O. A. Al-Owaedi, S. G. Eaves, D. C. Milan, M. Lemmer, B. W. Skelton, H. M. Osorio, R. J. Nichols, S. J. Higgins, P. Cea, N. J. Long, T. Albrecht, S. Martín, C. J. Lambert, P. J. Low, *Chem. - Eur. J.* **2017**, *23*, 2133.
- [10] O. A. Al-Owaedi, S. Bock, D. C. Milan, M.-C. Oerthel, M. S. Inkpen, D. S. Yufit, A. N. Sobolev, N. J. Long, T. Albrecht, S. J. Higgins, M. R. Bryce, R. J. Nichols, C. J. Lambert, P. J. Low, *Nanoscale* **2017**, *9*, 9902.
- [11] F. Schwarz, G. Kastlunger, F. Lissel, H. Riel, K. Venkatesan, H. Berke, R. Stadler, E. Lörtscher, *Nano Lett.* **2014**, *14*, 5932.

- [12] F. Schwarz, G. Kastlunger, F. Lissel, C. Egler-Lucas, S. N. Semenov, K. Venkatesan, H. Berke, R. Stadler, E. Lörtscher, *Nat. Nanotechnol.* **2016**, *11*, 170.
- [13] J.-C. Li, J.-Z. Wu, X. Gong, *J. Phys. Chem. Lett.* **2014**, *5*, 1017.
- [14] L. Luo, A. Benameur, P. Brignou, S. H. Choi, S. Rigaut, C. D. Frisbie, *J. Phys. Chem. C* **2011**, *115*, 19955.
- [15] K. S. Kumar, R. R. Pasula, S. Lim, C. A. Nijhuis, *Adv. Mater.* **2016**, *28*, 1824.
- [16] Z. Karipidou, B. Branchi, M. Sarpasan, N. Knorr, V. Rodin, P. Friederich, T. Neumann, V. Meded, S. Rosselli, G. Nelles, W. Wenzel, M. A. Rampi, F. von Wrochem, *Adv. Mater.* **2016**, *28*, 3473.
- [17] D. J. Wold, R. Haag, M. A. Rampi, C. D. Frisbie, *J. Phys. Chem. B* **2002**, *106*, 2813.
- [18] G. Kuang, S.-Z. Chen, W. Wang, T. Lin, K. Chen, X. Shang, P. N. Liu, N. Lin, *J. Am. Chem. Soc.* **2016**, *138*, 11140.
- [19] B. A. Friesen, B. Wiggins, J. L. McHale, U. Mazur, K. W. Hipps, *J. Am. Chem. Soc.* **2010**, *132*, 8554.
- [20] V. Kolivoška, M. Valášek, M. Gál, R. Sokolová, J. Bulíčková, L. Pospíšil, G. Mészáros, M. Hromadová, *J. Phys. Chem. Lett.* **2013**, *4*, 589.
- [21] L. Xiang, T. Hines, J. L. Palma, X. Lu, V. Mujica, M. A. Ratner, G. Zhou, N. Tao, *J. Am. Chem. Soc.* **2016**, *138*, 679.
- [22] S. Goswami, A. J. Matula, S. P. Rath, S. Hedström, S. Saha, M. Annamalai, D. Sengupta, A. Patra, S. Ghosh, H. Jani, S. Sarkar, M. R. Motapothula, C. A. Nijhuis, J. Martin, S. Goswami, V. S. Batista, T. Venkatesan, *Nat. Mater.* **2017**, *16*, 1216.
- [23] J.-H. Tang, T.-G. Sun, J.-Y. Shao, Z.-L. Gong, Y.-W. Zhong, *Chem. Commun.* **2017**, *53*, 11925.
- [24] Y.-P. Lin, C. H. Bennett, T. Cabaret, D. Vodenicarevic, D. Chabi, D. Querlioz, B. Jusselme, V. Derycke, J.-O. Klein, *Sci. Rep.* **2016**, *6*, 31932.
- [25] G. Lovat, B. Choi, D. W. Paley, M. L. Steigerwald, L. Venkataraman, X. Roy, *Nat. Nanotechnol.* **2017**, *12*, 1050.
- [26] T. L. Schull, J. G. Kushmerick, C. H. Patterson, C. George, M. H. Moore, S. K. Pollack, R. Shashidhar, *J. Am. Chem. Soc.* **2003**, *125*, 3202.
- [27] G. Sedghi, K. Sawada, L. J. Esdaile, M. Hoffmann, H. L. Anderson, D. Bethell, W. Haiss, S. J. Higgins, R. J. Nichols, *J. Am. Chem. Soc.* **2008**, *130*, 8582.
- [28] J. M. B. Kim, C. Olivier, S. Rigaut, D. Touchard, J. G. Kushmerick, X.-Y. Zhu, C. D. Frisbie, *J. Phys. Chem. C* **2007**, *111*, 7521.
- [29] N. Tuccitto, V. Ferri, M. Cavazzini, S. Quici, G. Zhavnerko, A. Licciardello, M. A. Rampi, *Nat. Mater.* **2009**, *8*, 41.
- [30] R. C. Bruce, R. Wang, J. Rawson, M. J. Therien, W. You, *J. Am. Chem. Soc.* **2016**, *138*, 2078.
- [31] Q. Ferreira, A. M. Bragança, L. Alcácer, J. Morgado, *J. Phys. Chem. C* **2014**, *118*, 7229.
- [32] K. Sugimoto, Y. Tanaka, S. Fujii, T. Tada, M. Kiguchi, M. Akita, *Chem. Commun.* **2016**, *52*, 5796.
- [33] S. Chappell, C. Brooke, R. J. Nichols, L. J. Kershaw Cook, M. Halcrow, J. Ulstrup, S. J. Higgins, *Faraday Discuss.* **2016**, *193*, 113.
- [34] R. Davidson, O. A. Al-Owaedi, D. C. Milan, Q. Zeng, J. Tory, F. Hartl, S. J. Higgins, R. J. Nichols, C. J. Lambert, P. J. Low, *Inorg. Chem.* **2016**, *55*, 2691.
- [35] O. A. Al-Owaedi, D. C. Milan, M.-C. Oerthel, S. Bock, D. S. Yufft, J. A. K. Howard, S. J. Higgins, R. J. Nichols, C. J. Lambert, M. R. Bryce, P. J. Low, *Organometallics* **2016**, *35*, 2944.
- [36] S. Hayami, Y. Komatsu, T. Shimizu, H. Kamihata, Y. H. Lee, *Coord. Chem. Rev.* **2011**, *255*, 1981.
- [37] S. Aroua, T. K. Todorova, P. Hommes, L.-M. Chamoreau, H.-U. Reissig, V. Mougel, M. Fontecave, *Inorg. Chem.* **2017**, *56*, 5930.
- [38] A. Bakkar, S. Cobo, F. Lafalet, D. Roldan, E. Saint-Aman, G. Royal, *J. Mater. Chem. C* **2016**, *4*, 1139.
- [39] C. Fave, Y. Leroux, G. Trippé, H. Randriamahazaka, V. Noel, J.-C. Lacroix, *J. Am. Chem. Soc.* **2007**, *129*, 1890.
- [40] C. Fave, V. Noel, J. Ghilane, G. Trippé-Allard, H. Randriamahazaka, J. C. Lacroix, *J. Phys. Chem. C* **2008**, *112*, 18638.
- [41] P. Martin, M. L. Della Rocca, A. Anthore, P. Lafarge, J.-C. Lacroix, *J. Am. Chem. Soc.* **2012**, *134*, 154.
- [42] V. Stockhausen, G. Trippé-Allard, N. Van Quynh, J. Ghilane, J.-C. Lacroix, *J. Phys. Chem. C* **2015**, *119*, 19218.
- [43] Q. van Nguyen, P. Martin, D. Frath, M. L. Della Rocca, F. Lafalet, C. Barraud, P. Lafarge, V. Mukundan, D. James, R. L. McCreery, J.-C. Lacroix, *J. Am. Chem. Soc.* **2017**, *139*, 11913.
- [44] M. Burgess, J. S. Moore, J. Rodríguez-López, *Acc. Chem. Res.* **2016**, *49*, 2649.
- [45] L. Cao, G. Fang, Y. Wang, *Langmuir* **2017**, *33*, 980.
- [46] Q. Van Nguyen, P. Martin, D. Frath, M. L. Della Rocca, F. Lafalet, S. Bellinck, P. Lafarge, J.-C. Lacroix, *J. Am. Chem. Soc.* **2018**, *140*, 10131.
- [47] C. Kahlfuss, E. Méta, M.-C. Duclos, M. Lemaire, A. Milet, E. Saint-Aman, C. Bucher, *Chem. - Eur. J.* **2015**, *21*, 2090.
- [48] V. Rabache, J. Chaste, P. Petit, M. L. Della Rocca, P. Martin, J.-C. Lacroix, R. L. McCreery, P. Lafarge, *J. Am. Chem. Soc.* **2013**, *135*, 10218.
- [49] D. Frath, V. Q. Nguyen, F. Lafalet, P. Martin, J.-C. Lacroix, *Chem. Commun.* **2017**, *53*, 10997.
- [50] M. Buda, G. Kalyuzhny, A. J. Bard, *J. Am. Chem. Soc.* **2002**, *124*, 6090.
- [51] B. Jusselme, G. Bidan, M. Billon, C. Goyer, Y. Kervella, S. Guillerez, E. A. Hamad, C. Goze-Bac, J.-Y. Mevellec, S. Lefrant, *J. Electroanal. Chem.* **2008**, *621*, 277.
- [52] V. Q. Nguyen, X. Sun, F. Lafalet, J.-F. Audibert, F. Miomandre, G. Lemerrier, F. Loiseau, J.-C. Lacroix, *J. Am. Chem. Soc.* **2016**, *138*, 9381.
- [53] C. Agnès, J.-C. Arnault, F. Omnès, B. Jusselme, M. Billon, G. Bidan, P. Mailley, *Phys. Chem. Chem. Phys.* **2009**, *11*, 11647.
- [54] C. A. Bessel, D. R. Rolison, *J. Phys. Chem. B* **1997**, *101*, 1148.
- [55] V. D. Chaube, S. Shylesh, A. P. Singh, *J. Mol. Catal. A: Chem.* **2005**, *241*, 79.
- [56] H. Yan, A. J. Bergren, R. McCreery, M. L. Della Rocca, P. Martin, P. Lafarge, J. C. Lacroix, *Proc. Natl. Acad. Sci. USA* **2013**, *110*, 5326.
- [57] S. Y. Sayed, J. A. Fereiro, H. Yan, R. L. McCreery, A. J. Bergren, *Proc. Natl. Acad. Sci. USA* **2012**, *109*, 11498.
- [58] S. H. Choi, B. Kim, C. D. Frisbie, *Science* **2008**, *320*, 1482.
- [59] S. H. Choi, C. Risko, M. C. R. Delgado, B. Kim, J.-L. Brédas, C. D. Frisbie, *J. Am. Chem. Soc.* **2010**, *132*, 4358.
- [60] T. Hines, I. Diez-Perez, J. Hihath, H. Liu, Z.-S. Wang, J. Zhao, G. Zhou, K. Müllen, N. Tao, *J. Am. Chem. Soc.* **2010**, *132*, 11658.
- [61] C. E. Smith, S. O. Odoh, S. Ghosh, L. Gagliardi, C. J. Cramer, C. D. Frisbie, *J. Am. Chem. Soc.* **2015**, *137*, 15732.
- [62] C. S. S. Sangeetha, A. T. Demissie, L. Yuan, T. Wang, C. D. Frisbie, C. A. Nijhuis, *J. Am. Chem. Soc.* **2016**, *138*, 7305.
- [63] D. Taherinia, C. E. Smith, S. Ghosh, S. O. Odoh, L. Balhorn, L. Gagliardi, C. J. Cramer, C. D. Frisbie, *ACS Nano* **2016**, *10*, 4372.
- [64] A. Morteza Najarian, R. L. McCreery, *ACS Nano* **2017**, *11*, 3542.
- [65] O. Ivashenko, A. J. Bergren, R. L. McCreery, *Adv. Electron. Mater.* **2016**, *2*, 1600351.
- [66] L. Yuan, L. Wang, A. R. Garrigues, L. Jiang, H. V. Annadata, M. Anguera Antonana, E. Barco, C. A. Nijhuis, *Nat. Nanotechnol.* **2018**, *13*, 322.
- [67] A. Migliore, P. Schiff, A. Nitzan, *Phys. Chem. Chem. Phys.* **2012**, *14*, 13746.
- [68] U. M. Tefashe, Q. Van Nguyen, A. Morteza Najarian, F. Lafalet, J.-C. Lacroix, R. L. McCreery, *J. Phys. Chem. C* **2018**, *122*, 29028.
- [69] J. Hankache, O. S. Wenger, *Chem. Rev.* **2011**, *111*, 5138.

- [70] J. C. Lacroix, K. I. Chane-Ching, F. Maquère, F. Maurel, *J. Am. Chem. Soc.* **2006**, *128*, 7264.
- [71] G. Sedghi, V. M. García-Suárez, L. J. Esdaile, H. L. Anderson, C. J. Lambert, S. Martín, D. Bethell, S. J. Higgins, M. Elliott, N. Bennett, J. E. Macdonald, R. J. Nichols, *Nat. Nanotechnol.* **2011**, *6*, 517.
- [72] J. A. Fereiro, X. Yu, I. Pecht, M. Sheves, J. C. Cuevas, D. Cahen, *Proc. Natl. Acad. Sci. USA* **2018**, *115*, E4577.
- [73] J. A. Fereiro, G. Porat, T. Bendikov, I. Pecht, M. Sheves, D. Cahen, *J. Am. Chem. Soc.* **2018**, *140*, 13317.
- [74] B. de Nijs, F. Benz, S. J. Barrow, D. O. Sigle, R. Chikkaraddy, A. Palma, C. Carnegie, M. Kamp, R. Sundararaman, P. Narang, O. A. Scherman, J. J. Baumberg, *Nat. Commun.* **2017**, *8*, 994.
- [75] J. C. Lacroix, *Curr. Opin. Electrochem.* **2018**, *7*, 153.
- [76] A. J. Bergren, L. Zeer-Wanklyn, M. Semple, N. Pekas, B. Szeto, R. L. McCreery, *J. Phys.: Condens. Matter* **2016**, *28*, 094011.